Chinese Journal of Natural Medicines

Silibinin meglumine ameliorates hepatic encephalopathy *via* inhibiting UCP2–mediated oxidative stress and mitochondrial dysfunction

Yue Li, Hong Chen, Xinyi Chen, Zhangqiu Zhou, Jieman Wang, Yuanyuan Zhang, Shengpeng Zhang, Hongliang He, Junping Kou

Citation: Yue Li, Hong Chen, Xinyi Chen, Zhangqiu Zhou, Jieman Wang, Yuanyuan Zhang, Shengpeng Zhang, Hongliang He, Junping Kou, Silibinin meglumine ameliorates hepatic encephalopathy *via* inhibiting UCP2–mediated oxidative stress and mitochondrial dysfunction, Chinese Journal of Natural Medicines, 2026, 24(5), 619–631. doi: 10.1016/S1875–5364(26)61180–6.

View online: https://doi.org/10.1016/S1875–5364(26)61180–6

Chinese Journal of Natural Medicines 24 (2026) 619-631

Contents lists available at ScienceDirect

Chinese Journal of Natural Medicines

journal homepage: www.cjnmcpu.com/

Original article

Silibinin meglumine ameliorates hepatic encephalopathy *via* inhibiting UCP2-mediated oxidative stress and mitochondrial dysfunction

Yue Li[a,Δ], Hong Chen[a,Δ], Xinyi Chen[a], Zhangqiu Zhou[a], Jieman Wang[a], Yuanyuan Zhang[a], Shengpeng Zhang[a,b], Hongliang He[c,*], Junping Kou[a,*]

[a] *State Key Laboratory of Natural Medicines, Jiangsu Key Laboratory of TCM Evaluation and Translational Research, Department of Pharmacology of Chinese Material Medica, School of Traditional Chinese Pharmacy, China Pharmaceutical University, Nanjing 211198, China*

[b] *School of Pharmacy, Wannan Medical College, Wuhu 241000, China*

[c] *Department of Pharmacy, Sir Run Run Hospital, Nanjing Medical University, Nanjing 211198, China*

ARTICLE INFO

Article history:
Received 14 September 2025
Revised 13 December 2025
Accepted 25 January 2026
Available online 20 May 2026

Keywords:
Hepatic encephalopathy
Silibinin meglumine
Uncoupling protein 2
Oxidative stress
Mitochondrial dysfunction
Mitophagy

ABSTRACT

Hepatic encephalopathy (HE) is a severe clinical condition with limited therapeutic options. Silybin, a principal bioactive constituent of milk thistle, is a natural compound known for its protective effects against various liver diseases and neurodegenerative disorders. Silibinin meglumine (SM), the meglumine salt of silybin, is widely used in the management of hepatic disorders. However, the therapeutic potential and mechanistic basis of SM in HE remain incompletely elucidated. In this study, SM reduced serum ammonia levels and improved hepatic function markers, including alanine transaminase, aspartate transaminase, and total bilirubin (TBil), in thioacetamide (TAA)-induced HE mice. SM also attenuated inflammatory cytokines such as tumor necrosis factor (TNF) and interleukin-6 (IL-6) in both plasma and brain tissue, reduced the oxidative stress marker malondialdehyde, and increased glutathione levels. Furthermore, molecular docking, cellular thermal shift assay (CETSA), drug affinity responsive target stability (DARTS) assay, and microscale thermophoresis (MST) assay collectively indicated that uncoupling protein 2 (UCP2) may serve as a direct molecular target of SM in mitigating HE. Notably, SM downregulated UCP2 expression in liver tissue and alleviated oxidative stress and mitochondrial dysfunction through modulation of the UCP2/PINK1/Drp1/mitofusin-2 (MFN2)/LC3B pathway. Additionally, co-administration of a UCP2 inhibitor partially attenuated the antioxidant effects of SM; however, no statistically significant reduction was observed in alanine aminotransferase (ALT) and aspartate aminotransferase (AST). In summary, this study demonstrates that SM-mediated targeting of UCP2 enhances hepatic mitochondrial function and suppresses excessive mitophagy, thereby ameliorating TBil in TAA-induced HE. These findings suggest that SM may represent a promising therapeutic strategy for TAA-induced HE.

1. Introduction

Hepatic encephalopathy (HE) is a central nervous system dysfunction resulting from acute or chronic severe liver injury [1]. The primary clinical manifestations include disturbances in consciousness, behavioral abnormalities, and, in severe cases, coma. These symptoms substantially impair quality of life and antioxidant response element (ARE) associated with increased mortality. Studies indicate that up to 40% of patients with cirrhosis develop HE within five years. However, specific and effective therapeutic options remain limited [2]. Therefore, identifying potential pharmacological agents that may ameliorate HE is critically important.

The pathogenesis of HE is multifactorial, involving toxin accumulation, metabolic disturbances, neurotransmitter imbalances, and oxidative stress [3]. A widely accepted mechanism is impaired ammonia metabolism due to compromised hepatic function, leading to systemic hyperammonemia and subsequent neurotoxicity. In HE, oxidative stress serves as a key pathway through which neurotoxins such as ammonia induce neuronal damage. The severity of HE correlates positively with elevated oxidative stress markers in patients with liver disease, suggesting that targeting oxidative stress may represent a pivotal therapeutic strategy [4].

Uncoupling protein 2 (UCP2), a mitochondrial inner membrane protein, modulates oxidative stress by regulating mitochondrial membrane potential and calcium ion homeostasis [5]. By reducing mitochondrial reactive oxygen species (ROS) production, UCP2 protects hepatocytes from oxidative injury, potentially mitigating the progression of liver disease. In alcoholic hepatitis, UCP2 is closely linked to disease progression, and evidence indicates that the UCP2 pathway attenuates oxidative stress, thereby exerting protective effects in alcohol-induced liver injury [6]. Additionally, UCP2 influences the development of alcoholic

* Corresponding author.
E-mail addresses: hhl725@ustc.edu.cn (H. He); junpingkou@cpu.edu.cn (J. Kou)
Δ These authors contributed equally to this work.

https://doi.org/10.1016/S1875-5364(26)61180-6

hepatitis through the regulation of fatty acid metabolism and insulin secretion. In non-alcoholic fatty liver disease (NAFLD), UCP2 expression may be altered by lipid accumulation, potentially modulating hepatic inflammation [7]. UCP2 also plays a significant role in regulating hepatocyte autophagy; studies suggest that UCP2 contributes to the pathogenesis of liver injury by modulating autophagic processes, particularly in the context of fatty acid-induced hepatocyte damage. These findings indicate that UCP2 not only mitigates oxidative stress but may also influence liver disease progression through autophagy regulation. Thus, targeting UCP2 represents a promising approach for alleviating liver injury across multiple etiologies. A deeper understanding of UCP2 function may therefore yield novel therapeutic strategies for HE [8].

Several natural compounds have demonstrated pharmacological potential in treating liver diseases. Silybin, a flavonolignan derived from milk thistle, exhibits significant therapeutic potential due to its antioxidant, anti-inflammatory, and anti-fibrotic properties [9]. However, silybin has low oral bioavailability, which limits its clinical utility. In contrast, its water-soluble derivative, silibinin meglumine (SM), is suitable for intravenous administration and has shown efficacy in improving liver function in murine models of liver fibrosis [10]. Nevertheless, definitive evidence regarding the potential of SM to ameliorate HE is currently lacking. Therefore, this study aims to investigate whether SM improves HE by targeting UCP2-mediated oxidative stress and mitochondrial dysfunction, thereby evaluating its therapeutic potential.

2. Material and methods

2.1. Drugs and reagents

Thioacetamide (TAA) was purchased from Sigma (Missouri, USA) and dissolved in sterile water. SM (≥ 98% purity) was obtained from Nanjing Chenxiang Biotechnology Co., Ltd. (Nanjing, China) and dispersed in sterile water to prepare SM solutions at concentrations of 0.5 mg·mL^{-1}, 0.25 mg·mL^{-1}, and 0.125 mg·mL^{-1}. Ornithine aspartate (OA) was purchased from Merz Pharmaceuticals GmbH (Frankfurt, Germany) and dispersed in sterile water to yield a 0.13 mg·mL^{-1} OA solution. Polyene phosphatidylcholine (PPC) was obtained from Chengdu Tiantaishan Pharmaceutical (Chengdu, China) and dispersed in sterile water to produce a 6.045 mg·mL^{-1} PPC solution. Genipin (GEN) was acquired from MCE (New Jersey, USA) and dispersed in sterile water to obtain a 0.5 mg·mL^{-1} GEN solution. Antibodies against PINK1, phosphorylated Drp1 (p-Drp1) (Ser616), Drp1, and mitofusin-2 (MFN2) were purchased from CST (1 ∶ 1000, Boston, MA, USA); anti-UCP2, anti-Iba1, and anti-GFAP antibodies were obtained from Abcam (1 ∶ 1000, Cambridge, UK); LC3B antibody was sourced from Proteintech (1 ∶ 500, Wuhan, China). Goat anti-mouse IgG H&L (HRP) and goat anti-rabbit IgG H&L (HRP) were purchased from Nanjing Bioworld Biotechnology Co., Ltd. (1 ∶ 10000, Nanjing, China). All antibodies were diluted according to the manufacturer' instructions. Mouse tumor necrosis factor α (TNF-α) and interleukin-1β (IL-1β) enzyme-linked immunosorbent assay (ELISA) kits were obtained from Nanjing Jin Yibai Biological Science and Technology Co., Ltd. (Nanjing, China). Alanine aminotransferase (ALT), aspartate aminotransferase (AST), total bilirubin (TBil), ammonia, glutathione (GSH), and malondialdehyde (MDA) activity assay kits were purchased from Nanjing Jiancheng Bioengineering Institute (Nanjing, China). Fluorescent probes DCFH-DA for ROS detection and Rhod-2 AM for mitochondrial calcium ions were acquired from Beyotime Biotechnology (Shanghai, China). UCP2 recombinant protein was obtained from Wuhan USCN Business Co., Ltd. (Wuhan, China). Monolith™ RED-NHS second-generation protein labeling kit was provided by NanoTemper Technologies (Munich, Germany).

2.2. Animals

All animal care and experimental procedures were conducted in accordance with the guidelines of the China National Institutes of Health and approved by the Animal Care and Use Committee of China Pharmaceutical University (approval number: 2024-11-145). Male C57BL/6J mice (22 ± 2 g) were supplied by Jiangsu Huachuang Sino Phar-maTech Co., Ltd. (Taizhou, Jiangsu, China, NO. A202401150332). Mice were housed under controlled conditions of temperature (23 ± 2 °C), humidity (50% ± 10%), and a 12-hour light/dark cycle, with free access to standard chow and water.

2.3. Animals and Treatments

2.3.1. Animal experiment 1: SM/OA/PPC treatment on TAA model

Mice were randomly assigned to seven groups (n = 8 per group): control group (normal saline), TAA group (200 mg·kg^{-1}), TAA + SM groups (SM at 1.25 mg·kg^{-1}, 2.5 mg·kg^{-1}, or 5 mg·kg^{-1}), TAA + OA group (1.3 mg·kg^{-1}), and TAA + PPC group (60.45 mg·kg^{-1}). Doses were determined based on conversion from human clinical dosages. HE was induced by intraperitoneal injection of TAA for two consecutive days. On the second day, SM was administered intravenously at the same time as TAA, once daily for three consecutive days, based on prior studies [11-15]. The positive control groups received OA or PPC *via* tail vein injection, while the remaining groups received an equivalent volume of saline. One hour after the final administration, behavioral tests were performed, followed by euthanasia. Blood, liver, and brain tissues were collected immediately. After centrifugation, supernatants were stored at −80 °C along with tissue samples.

2.3.2. Animal experiment 2: SM/ + GEN treatment experiment

Male C57BL/6J mice (22 ± 2 g) were randomly divided into five groups (n = 8 per group): control group, TAA group (200 mg·kg^{-1}), TAA + SM group (5 mg·kg^{-1}), TAA + GEN group (GEN, 2.5 mg·kg^{-1}), and TAA + SM + GEN group (5 mg·kg^{-1} + 2.5 mg·kg^{-1}). The experimental protocol followed the same TAA-induced model procedure as in experiment 1. Serum and liver samples were collected at the end of the treatment for further analysis. The dosage of GEN was selected based on a previous study [16].

2.4. Cell culture and treatment

HepG2 cells were obtained from the Chinese Academy of Sciences (Shanghai, China) and cultured in DMEM (Gibco, USA) supplemented with 10% fetal bovine serum (Gibco, USA) at 37 °C in a humidified atmosphere containing 5% CO_2. Cells were pretreated with 5 μmol·L^{-1} SM or 10 μmol·L^{-1} GEN for 30 minutes, followed by exposure to a solution containing D-GalN (5 μmol·L^{-1}) and LPS (1 μg·mL^{-1}) for 24 h to induce liver failure, as described in previous studies [17, 18].

2.5. Open field test in mice

The open field test was conducted in a square box (50 cm × 50 cm × 45 cm) with opaque plastic walls. The floor was divided into 25 equal sections (10 cm × 10 cm), with the 16 peripheral sections defined as the "fringe field" and the 9 central sections as the "center field". Prior to testing, each mouse was placed in the same starting position for a 5-minute acclimatization period. The test duration was 3 minutes, during which spontaneous locomotor activity was recorded using a video tracking system. Total distance traveled, distance moved in the center field, and total

activity time were automatically analyzed. After each trial, residual odors were removed by lightly spraying the floor with 70% alcohol and wiping it dry.

2.6. Analysis of biochemical indexes in serum and tissue

The levels of ALT, AST, TBil, and ammonia in mouse serum, as well as GSH and MDA contents in brain tissue homogenates, were measured according to the manufacturer's instructions.

2.7. Inflammatory factor detection

Serum and brain tissue levels of inflammatory cytokines were quantified using ELISA kits, following the manufacturer's protocols.

2.8. Liver histomorphology observation

Liver tissues were fixed in 10% formaldehyde, embedded in paraffin, and sectioned. Sections were stained with hematoxylin and eosin (H&E) to evaluate histopathological changes under light microscopy.

2.9. Molecular docking and molecular dynamics simulation

The three-dimensional structure of SM was retrieved from the PubChem database and converted to MOL2 format. Protein structures of UCP2, GRIN1, PTEN, GATM, ABAT, and PRKCD were downloaded from the Protein Data Bank (PDB). Molecular docking was performed using AutoDockTools to predict binding sites and calculate binding energies. Interactions between SM and UCP2 were further visualized and analyzed using PyMOL software to identify key amino acid residues involved in binding.

2.10. Immunohistochemistry and immunofluorescence

Paraffin-embedded sections (4 μm) were deparaffinized, rehydrated, subjected to antigen retrieval, and blocked prior to incubation with primary antibodies against UCP2, PINK1, MFN2, LC3B, and Iba1 overnight at 4 °C. Sections were then incubated with HRP-conjugated secondary antibodies at 37 °C for 30 minutes. After DAB staining and counterstaining with hematoxylin, images were captured under a light microscope. Densitometric analysis was performed using Image Pro Plus. For immunofluorescence, sections were permeabilized for 15 minutes, incubated with anti-GFAP antibody at 4 °C overnight, followed by secondary antibody incubation and DAPI staining. Fluorescence signals were visualized using a fluorescence microscope.

2.11. Western blotting (WB)

Proteins were extracted from mouse liver tissues using RIPA lysis buffer. Equal amounts of protein were separated by SDS-PAGE and transferred onto PVDF membranes. Membranes were incubated overnight at 4 °C with primary antibodies against UCP2, PINK1, Drp1, p-Drp1 (Ser616), MFN2, LC3B, Iba1, and GFAP. After washing, membranes were incubated with appropriate HRP-conjugated secondary antibodies for 1 h at room temperature. Protein bands were visualized using enhanced chemiluminescence reagents (Biosharp Co., Ltd., China) and detected with a ChemiDoc XRS + imaging system (Bio-Rad, USA).

2.12. Measurement of ROS and mitochondrial calcium ion level

Intracellular ROS levels were measured using the DCFH-DA probe, and mitochondrial calcium levels were assessed using Rhod-2 AM, according to the manufacturer's instructions.

2.13. Cellular thermal shift assay (CETSA)

HepG2 cell lysates were prepared by centrifugation at 12000 g for 15 minutes at 4 °C. SM (40 μmol·L^{-1}) or DMSO (vehicle control) was added to the supernatant and incubated at 4 °C. The samples were divided into eight aliquots and heated from 37 °C to 72 °C in 5 °C increments for 10 minutes each. After heating, samples were immediately cooled to −20 °C. Following a second centrifugation at 13 000 g for 15 minutes at 4 °C, the supernatants were collected for WB analysis.

2.14. Drug affinity responsive target stability (DARTS)

HepG2 cells were harvested and incubated with varying concentrations of SM (40, 20, 10, 5, 2.5 μmol·L^{-1}) at 4 °C for 3 hours. Cells were then lysed for 30 minutes and centrifuged at 12 000 g at 4 °C. Sample buffer was added, and samples were heated at 100 °C for 10 minutes prior to WB analysis.

2.15. Microscale thermophoresis (MST)

UCP2 recombinant protein was labeled using the Monolith™ RED-NHS second-generation protein labeling kit and diluted to 100 nmol·L^{-1} in 200 μL buffer for subsequent use. Based on preliminary data and expected Kd values, SM was serially diluted in two-fold steps to generate 16 concentrations. Each drug dilution was mixed with 10 μL of labeled protein (1 ∶ 1 ratio) and loaded into premium-coated capillaries. Capillaries were inserted into the capillary tray of the Monolith™ NT.115 instrument, and fluorescence was measured during capillary scanning. MST measurements were then initiated to assess binding affinity.

2.16. Statistical analysis

Data were analyzed using GraphPad Prism 8.0 software (GraphPad Software, USA). Differences between two groups were assessed using a two-tailed Student's *t*-test. For multiple comparisons, one-way ANOVA followed by Dunnett's post hoc test was applied. Results are expressed as mean ± SEM. A P-value < 0.05 was considered statistically significant.

3. Results

3.1. SM ameliorated TAA-induced movement disorder in mice

The drug administration protocol is illustrated in Fig. 1A. The effects of SM on behavioral outcomes in TAA-induced HE mice were evaluated. As shown in Fig. 1B, TAA-HE mice exhibited significant deterioration in motor function. To further assess the effect of SM on central nervous system motor activity, an open field test was performed. TAA-treated mice displayed slow movement, lethargy, and depressive-like behavior, with activity restricted to the peripheral zone. In contrast, SM treatment increased the duration spent in the central zone (Fig. 1C) and total travel distance (Fig. 1D). These findings indicate that SM effectively ameliorated TAA-induced movement disorders.

3.2. SM ameliorated TAA-induced liver injury in mice

The impact of SM on hepatic function was examined in TAA-induced mice. As shown in Fig. 2, TAA-HE mice exhibited marked impairment in liver function, with elevated levels of ALT (Fig. 2A), AST (Fig. 2B), TBil (Fig. 2C), and blood ammonia (Fig. 2D). SM intervention significantly reduced the levels of these markers. Additionally, ELISA quantification revealed that TNF-α (Fig. 2E) and IL-1β (Fig. 2F) were significantly elevated in the TAA group

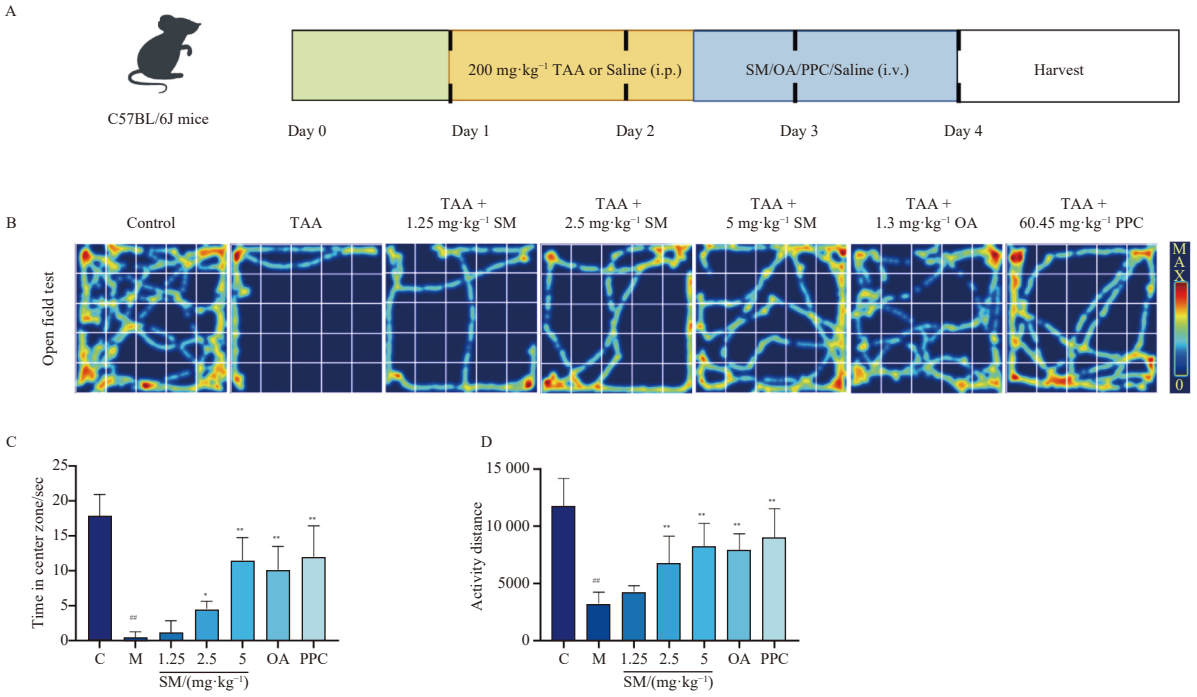

Fig. 1 SM attenuated TAA-induced HE-related pathological phenotypes in mice. (A) Schematic diagram of the establishment of the TAA-induced HE mouse model and the drug intervention schedule. (B) Representative movement trajectories in the open field test. (C) Time spent in the central zone. (D) Total travel distance (n = 4–6). Data are shown as mean ± SEM. $^{\#\#}P < 0.01$ *vs* normal group, $^{*}P < 0.05$, $^{**}P < 0.01$ *vs* Model group.

compared to controls, whereas SM treatment markedly lowered their levels. Macroscopic examination Fig. 2G showed that control livers were reddish, soft, and smooth, whereas HE group livers were hard, rough, swollen, and congested. SM treatment reduced hepatic congestion and swelling, with the SM (5 mg·kg^{-1}) group showing significantly less hemorrhage. H&E staining (Fig. 2H) demonstrated that SM reduced liver tissue necrosis, cellular swelling, and inflammatory cell infiltration compared to the HE group. These results indicate that SM effectively mitigated TAA-induced liver injury.

3.3. SM ameliorated TAA-induced oxidative stress and brain inflammation in mice

To evaluate the neuroprotective effects of SM in TAA-induced mice, oxidative stress and inflammatory markers in brain tissue were assessed. Biochemical analyses revealed that SM (2.5 mg·kg^{-1}, 5 mg·kg^{-1}) enhanced GSH activity (Fig. 3A) and reduced MDA content (Fig. 3B) compared to the TAA group. Furthermore, ELISA analysis of brain tissue showed significantly elevated levels of TNF-α, IL-1β, and IL-6 (Figs. 3C–3E) in the TAA group, which were markedly reduced in the SM group. Histological examination revealed neuronal disorganization and structural disarray in the hippocampal region of TAA mice, with evidence of degeneration and nuclear pyknosis. The number of degenerated or hyperchromatic neurons was reduced in both SM-treated groups, with the SM (5 mg·kg^{-1}) group showing a pronounced improvement in hippocampal neuroinflammation and neuronal morphology resembling that of the control group (Fig. 3F). Overall, SM intervention reduced pro-inflammatory cytokine levels in brain tissue, suggesting its potential role in alleviating HE.

3.4. SM inhibited TAA-induced activation of microglia in the brain tissue of mice

Iba1 is a microglia-specific marker protein. Immunohistochemical staining for Iba1 was used to detect changes in the number and morphology of microglia in the hippocampus and cortex, thereby assessing microglial activation. Control mice exhibited minimal microglia in cortical (Fig. 4A) and hippocampal regions (Fig. 4B), with sparse distribution. Statistical analysis revealed that the SM group had fewer activated microglia than the TAA group (Figs. 4C and 4D). Iba1 protein levels were significantly higher in the TAA group compared to controls (Fig. 4E). SM treatment (5 mg·kg^{-1}) notably reduced Iba1 levels, a finding supported by both immunohistochemistry and immunoblotting. SM also restored microglial morphology in the hippocampus and cortex of HE mice, limited microglial and astrocyte activation, and reduced the risk of brain edema.

3.5. SM inhibited TAA-induced activation of astrocytes in the brain tissue of mice

Given the critical role of astrocytes in neuroinflammation, the effect of SM on astrocyte activation was investigated in the TAA-induced HE model. Glial fibrillary acidic protein (GFAP) expression was analyzed by immunofluorescence and immunoblotting to assess astrocyte activation. In the control group, hippocampal astrocytes were sparse with weak GFAP fluorescence. In contrast, the TAA group exhibited increased astrocyte numbers, enhanced branching, and stronger GFAP fluorescence (Figs. 5A and 5B) and protein expression (Fig. 5C). SM treatment reduced astrocyte activation in the hippocampus, suggesting neuroprotective effects, attenuation of neuroinflammation, and prevention of brain dysfunction.

3.6. UCP2 might be a potential target mediating the protective effects of SM against HE

A network pharmacology approach was employed to elucidate the mechanism by which SM inhibits oxidative stress and improves HE. Fig. 6A shows that 61 potential silibinin targets were identified *via* the HERB database, and 944 HE-related targets were retrieved from the GeneCards database. Venn diagram analysis identified six overlapping targets: UCP2, GRIN1 [19], PTEN [20,21], GATM [22,23], ABAT [24], and PRKCD [25]. Molecular docking was performed to compare the binding affinity of silibinin (SM) to these six proteins. The results showed the highest interaction af-

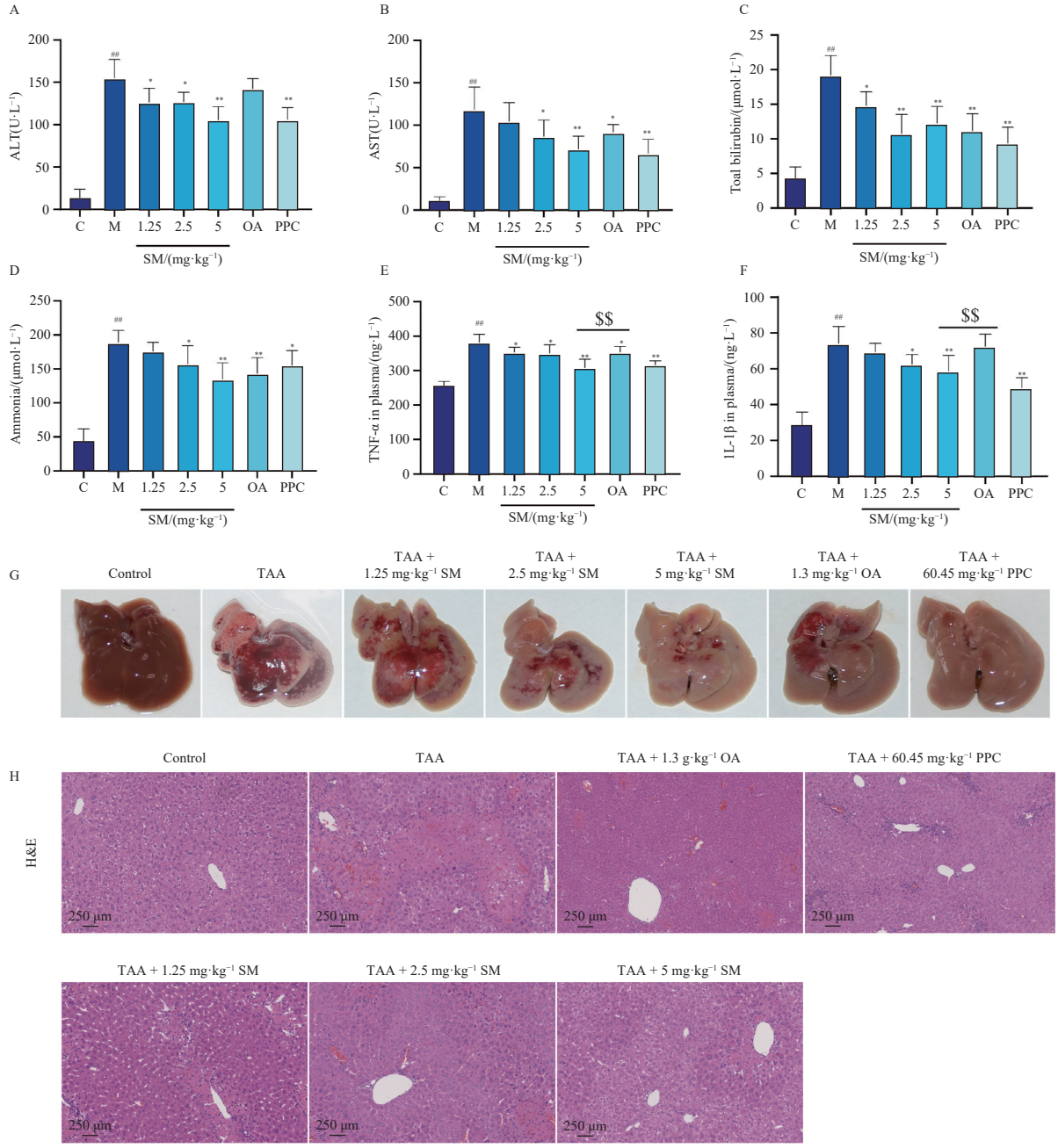

Fig. 2 SM mitigated TAA-induced liver injury in mice. (A–D) Serum ALT, AST, total bilirubin, and ammonia levels were measured by biochemical assays (n = 6). (E–F) Plasma TNF-α and IL-1β levels were measured in mice (n = 6). (G) Gross appearance of the livers (n = 3). (H) H&E staining of liver tissues (Scale bar = 250 μm) (n = 3). Data are shown as mean ± SEM. $^{\#\#}P < 0.01$ *vs* normal group, $^{*}P < 0.05$, $^{**}P < 0.01$ *vs* Model group, $^{\$\$}P < 0.01$ *vs* SM group (5 mg·kg^{-1}).

finity between silibinin and UCP2, with an average binding energy of −8.51 ± 0.2 kcal·mol^{-1} (Fig. 6B), binding to residues TYP100, ASN190, and PHE92 (Figs. 6C and 6D). The UCP2-silibinin complex exhibited stable root mean square deviation (RMSD) and root mean square fluctuation (RMSF) during molecular dynamics simulation (Figs. 6E and S1A). The binding affinity was further confirmed by CETSA and DARTS. CETSA demonstrated that SM treatment increased UCP2 protein expression under identical temperature conditions compared to the DMSO control (Fig. 6F). DARTS results indicated that increasing SM concentration enhanced UCP2 stability (Fig. 6G). MST analysis revealed a dissociation constant (Kd) of 1.583 ± 0.587 μmol·L^{-1} for the SM–UCP2 interaction (Figs. 6H and S1B-1I). These results demonstrate that SM exhibits significant binding affinity for UCP2, providing preliminary evidence that UCP2 may be a potential therapeutic target for SM in HE.

3.7. SM improved TAA-induced HE via the UCP2/PINK1/Drp1/MFN2/LC3B pathway in mice

The protective effects of SM against TAA-induced liver injury and neurological damage have been established, prompting further investigation into the underlying mechanisms. Oxidative stress is a key pathological mechanism in HE, capable of inducing mitochondrial dysfunction and triggering mitophagy. WB analysis showed that, compared to the TAA group, SM treatment reduced protein expression of UCP2 (Fig. 7A), PINK1 (Fig. 7B), p-Drp1 (Fig. 7C), and LC3B (Fig. 7E). Concurrently, MFN2 expression was upregulated (Fig. 7D). Immunohistochemical analysis of UCP2, PINK1, MFN2, and LC3B (Figs. 7F–7J) corroborated the WB findings. Collectively, these results indicate that SM inhibits mitophagy through the UCP2/PINK1/Drp1/MFN2/LC3B pathway, thereby alleviating TAA-induced HE.

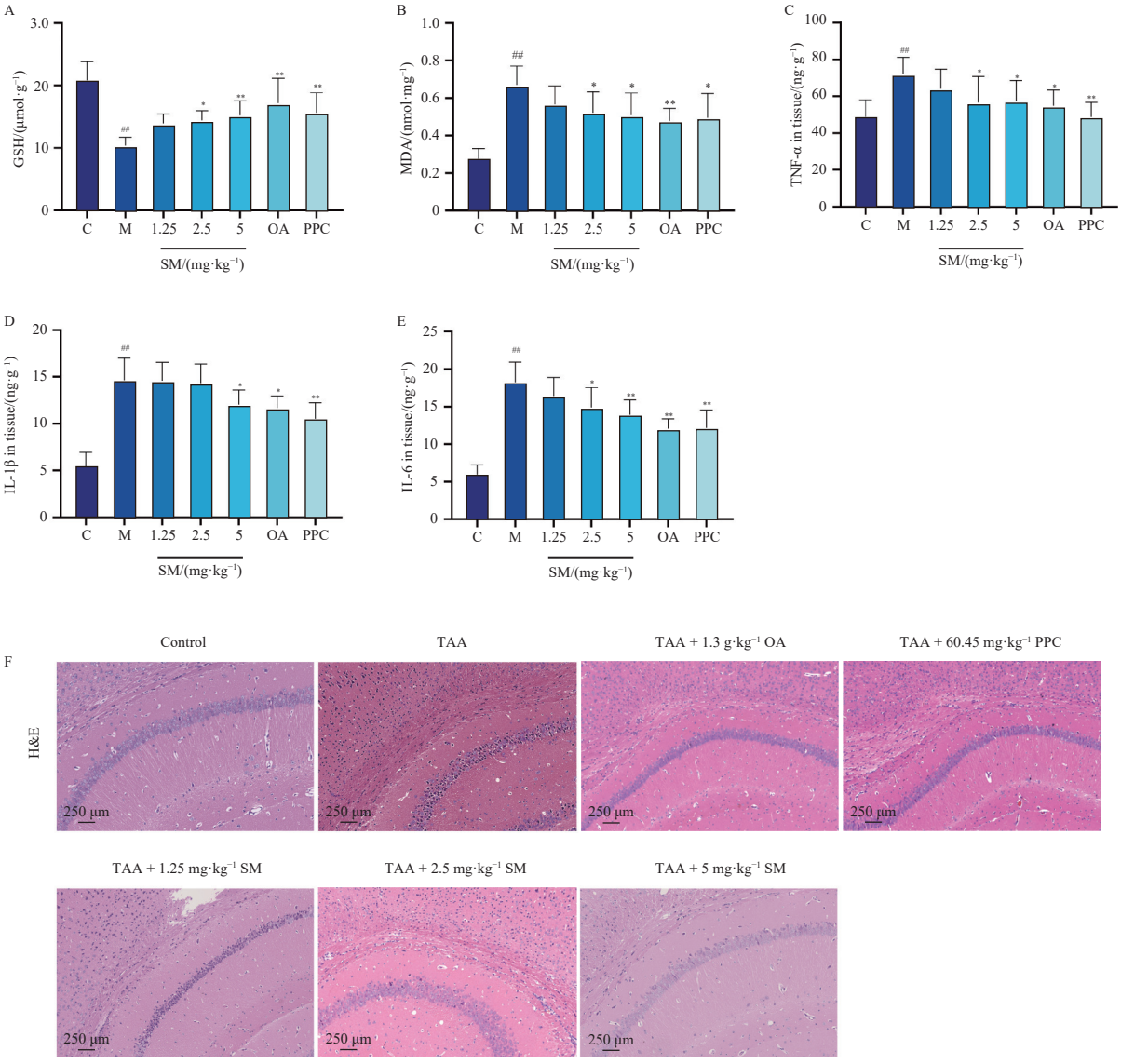

Fig. 3 SM ameliorated TAA-induced brain tissue injury in mice. (A–B) GSH and MDA levels in brain tissue homogenates were measured by biochemical assays (n = 6). (C–E) TNF-α, IL-1β, and IL-6 levels in mouse brain tissue homogenates were measured (n = 6). (F) H&E-stained hippocampal sections from different groups were examined under a light microscope (Scale bar = 250 μm) (n = 3). Data are shown as mean ± SEM. $^{\#\#}P$ <0.01 *vs* normal group, $^{*}P$ < 0.05, $^{**}P$ < 0.01 *vs* Model group.

3.8. The UCP2 inhibitor partially attenuated the antioxidant effects of SM in TAA-induced mice

To further investigate whether SM exerts its effects *via* UCP2, GEN, a UCP2 inhibitor, was employed. As shown, both GEN and SM reduced ALT (Fig. 8A), AST (Fig. 8B), and blood ammonia levels (Fig. 8F), improved oxidative stress markers (Figs. 8C–8E), and downregulated UCP2 (Fig. 8G), PINK1 (Fig. 8H), p-Drp1 (Fig. 8I), and LC3B (Fig. 8K), while upregulating MFN2 (Fig. 8J). Compared to the SM group, co-administration of SM and GEN reduced the increase in GSH content from 50.19% to 17.29% and in SOD content from 24.28% to 5.76%. The inhibition of MDA content decreased from 37.12% to 29.90%, and blood ammonia inhibition declined from 54.18% to 38.61%. These findings indicate that

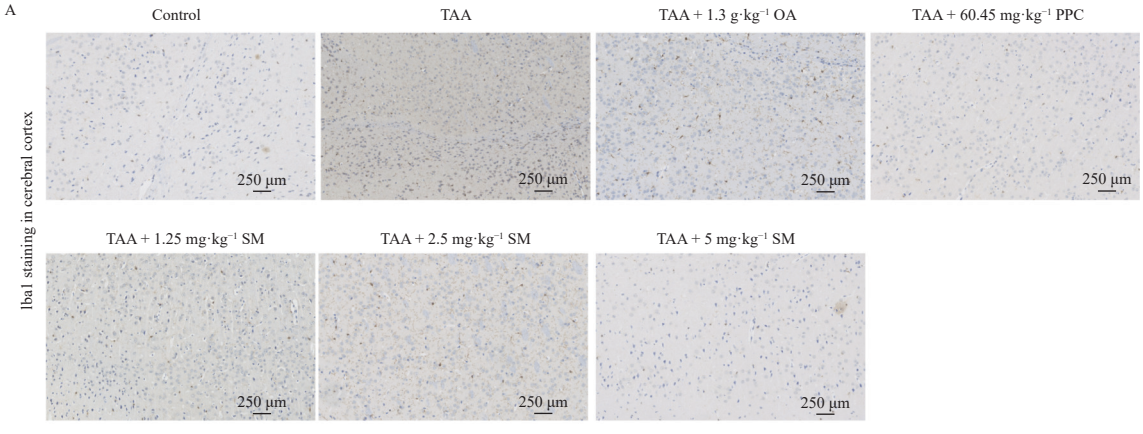

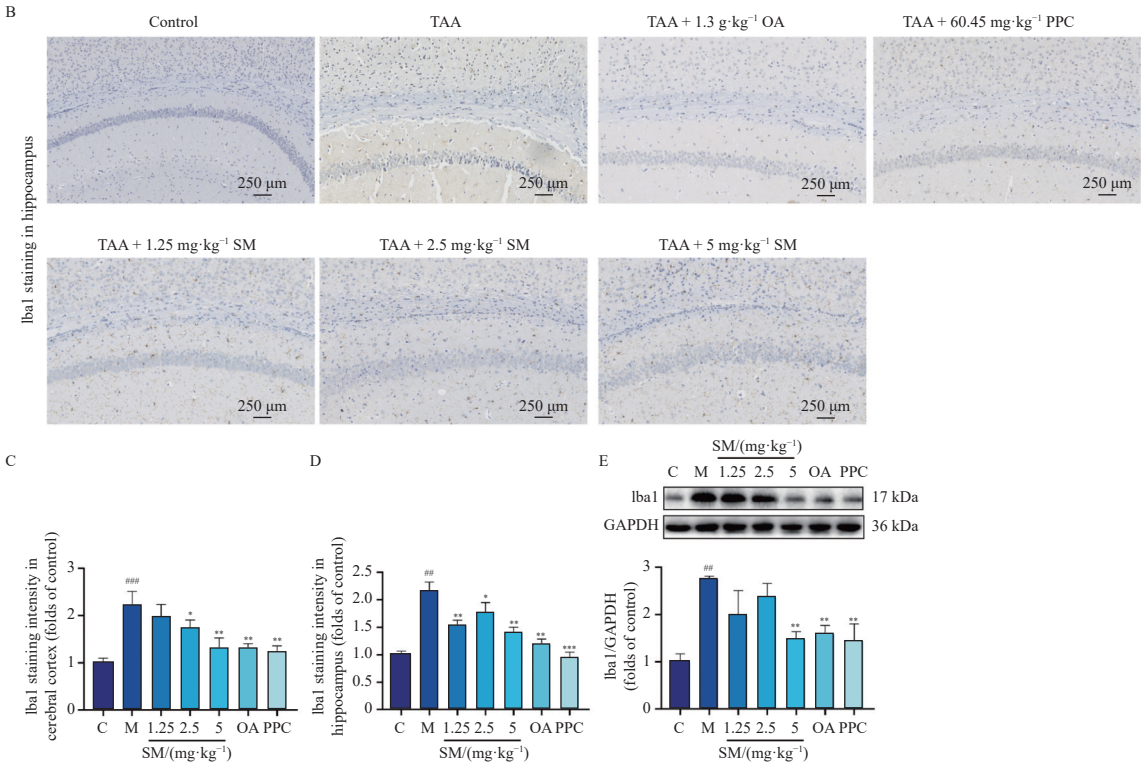

Fig. 4 SM inhibited TAA-induced microglial activation in mouse brain tissue. (A) Representative immunohistochemical images of Iba1 expression in the cerebral cortex (Scale bar = 250 μm) (n = 3). (B) Representative immunohistochemical images of Iba1 expression in the hippocampus (Scale bar = 250 μm) (n = 3). (C–D) Quantitative immunohistochemical analysis of Iba1 expression in the cerebral cortex and hippocampus (n = 3). (E) Western blot analysis of Iba1 in brain tissue homogenates (n = 3). Data are shown as mean ± SEM. $^{\#\#}P$ <0.01 *vs* normal group, $^{*}P$ < 0.05, $^{**}P$ < 0.01 *vs* Model group.

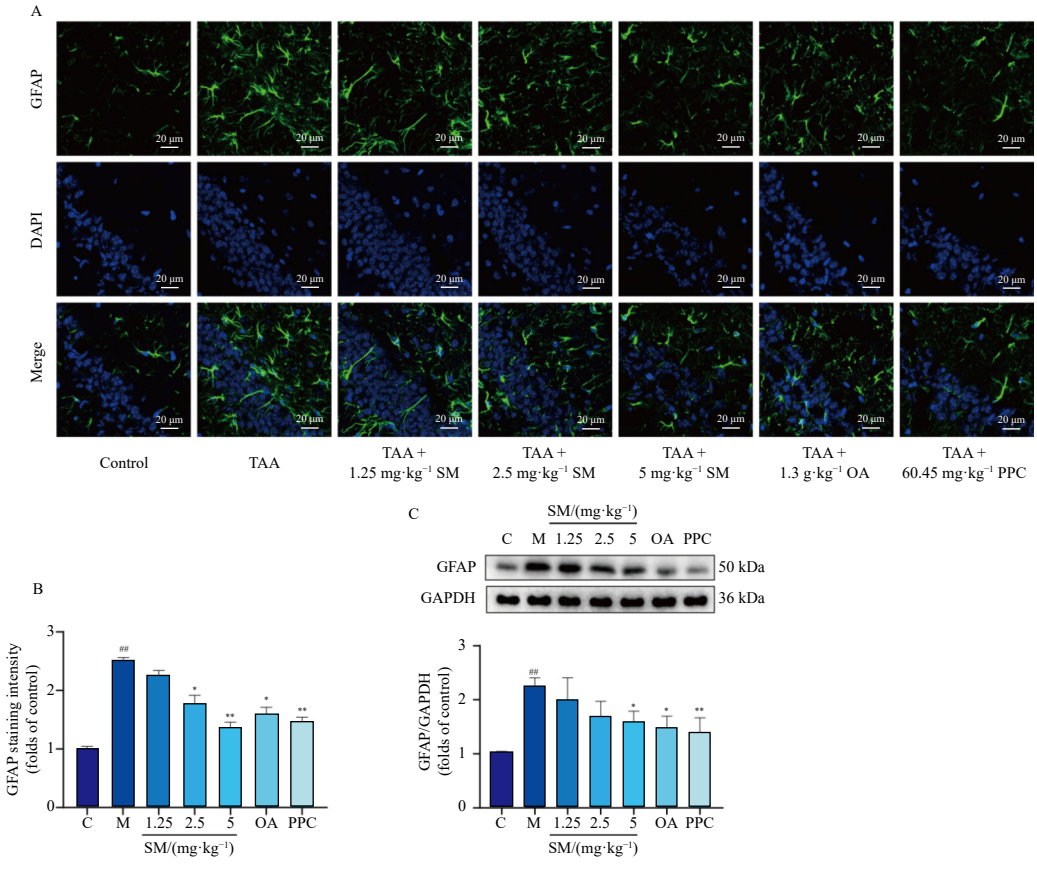

Fig. 5 SM suppressed the activation of astrocytes in mouse brain tissue. (A) Representative immunofluorescence images of GFAP expression (Scale bar= 20 μm) (n = 3). (B) Quantitative immunofluorescence analysis of GFAP staining intensity in the hippocampus (n = 3). (C) Western blot analysis of GFAP in brain tissue homogenates (n = 3). Data are shown as mean ± SEM. $^{\#\#}P$ <0.01 *vs* normal group, $^{*}P$ < 0.05, $^{**}P$ < 0.01 *vs* Model group.

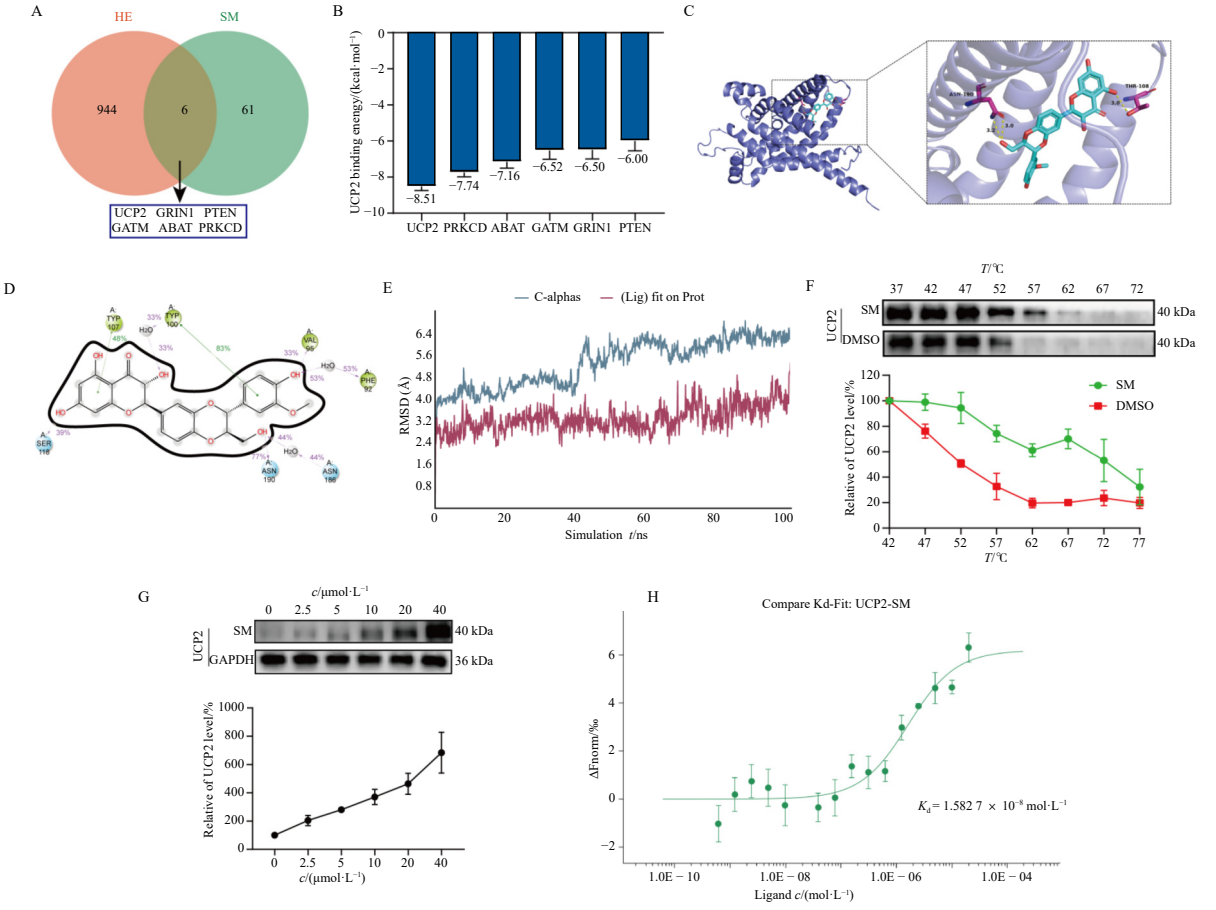

Fig. 6 UCP2 may represent a potential target through which SM alleviates HE. (A)Potential targets involved in the protective effect of silibinin against HE were screened using a Venn diagram based on HREB and GeneCards databases. (B) The binding affinities of silibinin toward six candidate proteins were compared based on molecular docking results. (C) Molecular docking model of silibinin with UCP2. (D) Predicted binding site between silibinin and UCP2. (E) The UCP2–silibinin complex exhibited stable RMSD values during the simulation. (F) CETSA analysis of SM and UCP2 (n = 3). (G) DARTS analysis of SM and UCP2 (n = 3). (H) The binding affinity between SM and UCP2 was examined by MST (n = 4).

GEN was particularly sensitive to changes in oxidative stress markers, further supporting a functional link between UCP2 and oxidative stress. Immunohistochemistry results (Figs. 8L–8P) corroborated the WB data, demonstrating that SM inhibits mitophagy by downregulating UCP2, thereby mitigating TAA-induced HE.

3.9. The UCP2 inhibitor partially attenuated the mitochondrial protective effects of SM in vitro

To further examine the role of UCP2 in mitochondrial dysfunction and the protective effects of SM, UCP2 inhibitors were used to suppress UCP2 expression in HepG2 cells *in vitro*. Compared to the D-galactosamine/lipopolysaccharide (DGalN/LPS) group, both SM and the inhibitor group reduced ALT (Fig. 9A) and AST (Fig. 9B) levels; however, the inhibitory effect of SM on these markers was diminished in the inhibitor group. Immunofluorescence analysis of ROS levels (Fig. 9C) revealed that SM reduced ROS, but this effect was partially reversed in the UCP2 inhibition group (Fig. 9D). Similarly, SM suppressed mitochondrial calcium release, but this effect was partially reversed upon UCP2 inhibition (Fig. 9E). WB analysis showed that UCP2 expression increased following DGalN/LPS stimulation but decreased after SM treatment. The UCP2 inhibitor also reduced UCP2 levels, and in this context, SM's suppressive effect on UCP2 was partially diminished (Fig. 9F). SM inhibited the upregulation of p-Drp1 under DGalN/LPS stimulation, but this inhibition was partially attenuated by the UCP2 inhibitor (Fig. 9G). These results suggest that the UCP2 inhibitor counteracts SM-induced reductions in ROS and mitochondrial calcium, as well as p-Drp1 downregulation, thereby reversing SM's protective effects against mitochondrial dysfunction. This further supports a role for SM in mitigating mitochondrial dysfunction, potentially mediated through UCP2.

4. Discussion

The liver plays a crucial role in metabolic production and detoxification, which are vital for maintaining systemic health. Hepatic dysfunction can lead to both systemic and liver-specific diseases, contributing significantly to the global burden of disease [26, 27]. Numerous herbal medicines have demonstrated efficacy in liver protection, with high safety profiles and minimal side effects [28]. Silybin, a natural polyphenol, exhibits diverse biological and pharmacological activities and is widely used globally as a hepatoprotective agent due to its anti-inflammatory, anti-lipid peroxidative, and anti-fibrotic properties [29]. However, the role of silybin in HE has not been previously reported. This study aimed to investigate the therapeutic effects and underlying mechanisms of SM, a meglumine salt of silybin with enhanced solubility and minimal cytotoxicity, in HE. We found that SM significantly ameliorates HE in both *in vivo* and *in vitro* models, particularly through modulation of UCP2, as well as its anti-oxidative and mitochondrial protective effects.

Previous studies have shown that silybin activates Nrf2 by promoting its nuclear translocation and binding to the ARE, thereby upregulating antioxidant gene expression and reducing hepatic oxidative stress [30]. Recent evidence indicates that silybin reduces ROS, mitigates oxidative stress-induced cell damage, and attenuates liver fibrosis progression [31]. These findings highlight silybin as a potent antioxidant with multi-level protective mech-

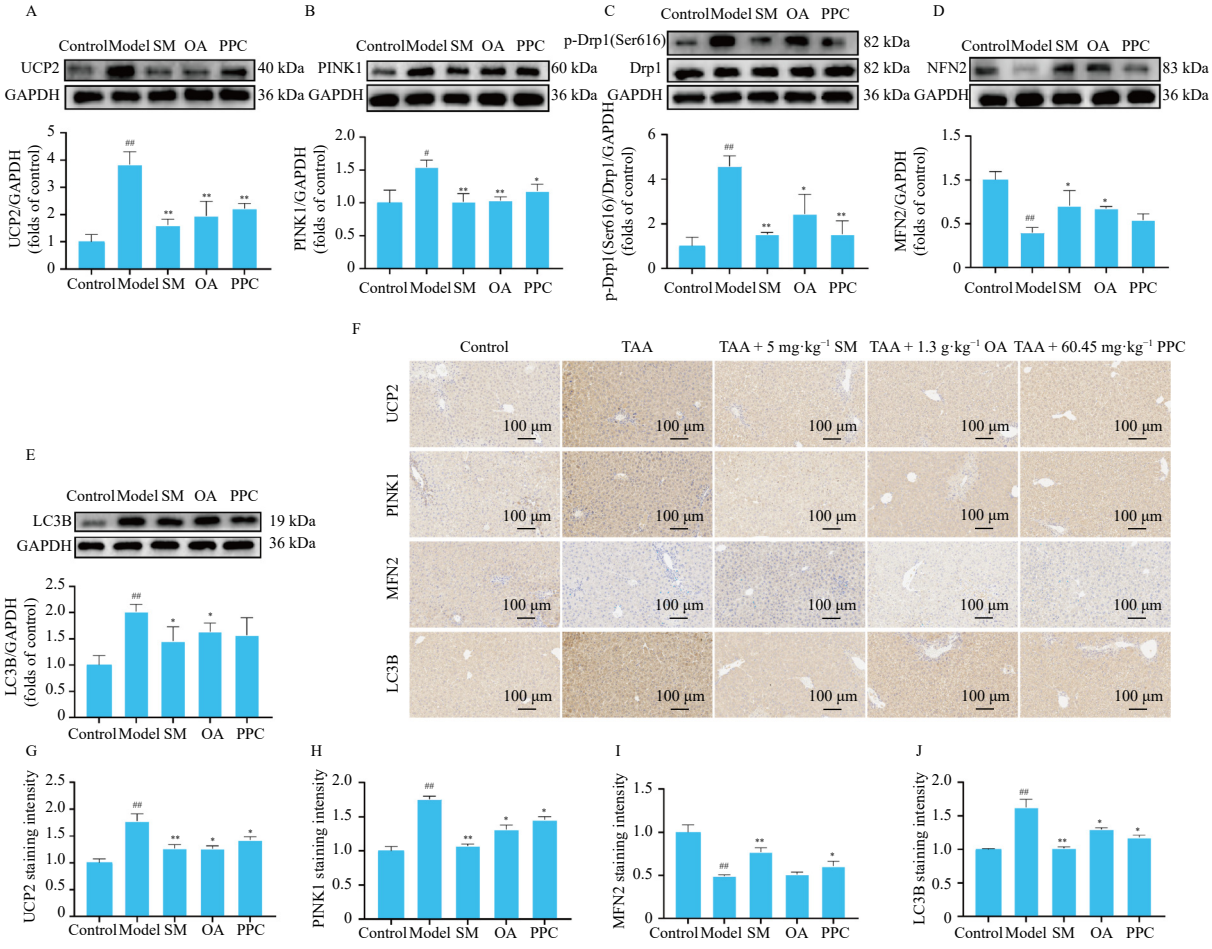

Fig. 7 SM alleviated TAA-induced HE *via* the UCP2/PINK1/Drp1/MFN2/LC3B pathway in mice. (A–E) Protein expression levels of UCP2, PINK1, p-Drp1, MFN2, and LC3B in liver tissues were quantitatively analyzed by Western blot (n = 3). (F–J) Protein expression levels of UCP2, PINK1, MFN2, and LC3B in liver tissues were quantitatively analyzed by immunohistochemistry (Scale bar =100 μm) (n = 3). Data are shown as mean ± SEM. $^{\#\#}P$ <0.01 *vs* normal group, $^{*}P$ < 0.05, $^{**}P$ < 0.01 *vs* Model group.

anisms, particularly in oxidative stress-related liver diseases [32]. Despite its broad therapeutic potential, silybin's clinical utility in severe conditions is limited by its low bioavailability [33]. SM partially overcomes this limitation through improved solubility. TAA is a well-characterized model for HE research, as it is metabolized into toxic intermediates, TAA sulphoxide and sulphone, inducing liver injury, impairing ammonia metabolism, and leading to hyperammonemia, oxidative stress, neurotoxicity, and metabolic disturbances [34, 35 8, 36]. In this study, wee valuated the therapeutic effects of SM in the TAA-induced HE model and elucidated its mechanisms of action. Spontaneous locomotor activity and exploratory behavior in mice demonstrated that SM effectively mitigates behavioral abnormalities associated with HE (Figs. 1B–1D). Moreover, SM treatment improved liver function compared to the TAA model (Figs. 2A–2C), significantly reduced blood ammonia levels (Fig. 2D), and alleviated hepatic pathological damage (Figs. 2G and 2H). Given that oxidative stress inhibition is critical in HE amelioration [37], we assessed oxidative stress markers and found that SM restored levels of MDA, SOD, and GSH in liver tissue (Figs. 3A and 3B). Additionally, SM reduced pro-inflammatory cytokines such as TNF-α and IL-1β in both liver (Figs. 2E and 2F) and brain tissues (Figs. 3C and 3D). Histological examination revealed a marked increase in astrocytes and cellular degeneration in the hippocampus of TAA-treated mice (Fig. 3F), which was significantly reversed by SM treatment. Concurrently, SM reduced GFAP protein expression in brain tissue (Fig. 5C), suggesting that it inhibits astrocyte activation and cytotoxic swelling (Fig. 5A) by lowering blood ammonia and suppressing neuroinflammation. These findings indicate that SM improves HE primarily by enhancing liver function, reducing circulating ammonia and other toxins, and attenuating peripheral inflammation, thereby diminishing neuroinflammation (Figs. 4A–4E). Collectively, SM ameliorates liver and brain pathology, oxidative stress, and inflammation, supporting its potential as a therapeutic agent for HE. Further validation in bile-duct ligation (BDL)-induced HE models could strengthen these findings.

Recent studies have established oxidative stress as a key contributor to HE, and its reduction has been shown to improve outcomes in various liver disorders [38-41], suggesting that targeting oxidative stress may be a viable therapeutic strategy. Using network pharmacology, we identified six potential protein targets of SM in HE (Figs. 6A and 6B). Among these, GRIN1 is associated with autophagy, PTEN regulates this process, GATM modulates oxidative stress and ferroptosis, ABAT is linked to neurological disorders, and PRCKD influences mitophagy. Notably, UCP2 has recently been proposed as a potential therapeutic target in HE. Therefore, we focused on elucidating the role of UCP2 in SM-mediated protection against TAA-induced HE, particularly through suppression of oxidative stress and mitochondrial dysfunction. UCP2, located in the inner mitochondrial membrane [42], regulates intracellular energy metabolism and oxidative stress [43]. By reducing mitochondrial ROS production, UCP2 helps mitigate oxidative damage, making it a promising target in HE. Thus, we investigated whether SM exerts its protective effects *via* UCP2 modulation. Our results showed that SM treatment reduced MDA levels and enhanced GSH activity in TAA-HE mouse tissues, indicating significant alleviation of oxidative stress. Molecular docking and molecular dynamics simulations confirmed a high binding affin-

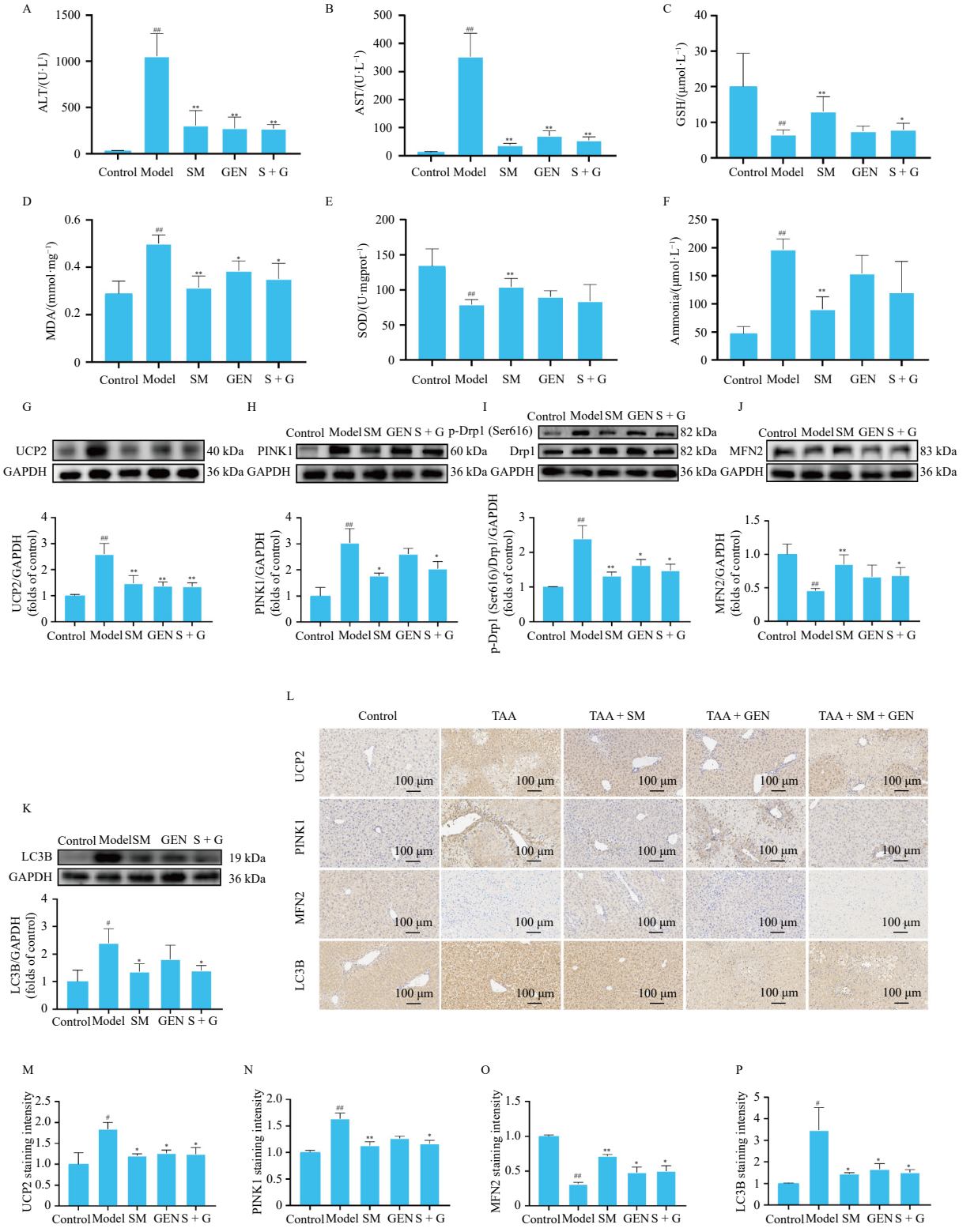

Fig. 8 The UCP2 inhibitor genipin and SM effectively mitigated TAA-induced HE in mice. (A–F) Serum ALT, AST, GSH, MDA, SOD, and ammonia levels were measured by biochemical assays (n = 6). (G–K) Protein expression levels of UCP2, PINK1, p-Drp1, MFN2, and LC3B in liver tissues were quantitatively analyzed by Western blot (n = 3). (L–P) Protein expression levels of UCP2, PINK1, MFN2, and LC3B in liver tissues were quantitatively analyzed by immunohistochemistry (Scale bar = 100 μm) (n = 3). Data are shown as mean ± SEM. $^{\#}P$ <0.05, $^{\#\#}P$ <0.01 *vs* normal group, $^{*}P$ < 0.05, $^{**}P$ < 0.01 *vs* Model group.

ity between SM and UCP2 (Figs. 6C-6E). CETSA and DARTS assays (Figs. 6F and 6G) further validated the stability of this interaction, while MST analysis yielded a Kd value of 1.583 ± 0.587 μmol·L^{-1}, confirming direct binding (Fig. 6H). These findings suggest that SM directly targets UCP2 to suppress oxidative stress. Further mechanistic studies, including the use of UCP2 knockout models, are warranted to fully elucidate this pathway. While this study focused on UCP2 due to its established role in redox regulation and mitophagy, additional targets may contribute to SM's therapeutic effects and merit future investigation.

Accumulating evidence indicates that ammonia induces ROS formation and elevates oxidative stress [44]. In turn, mild oxidative

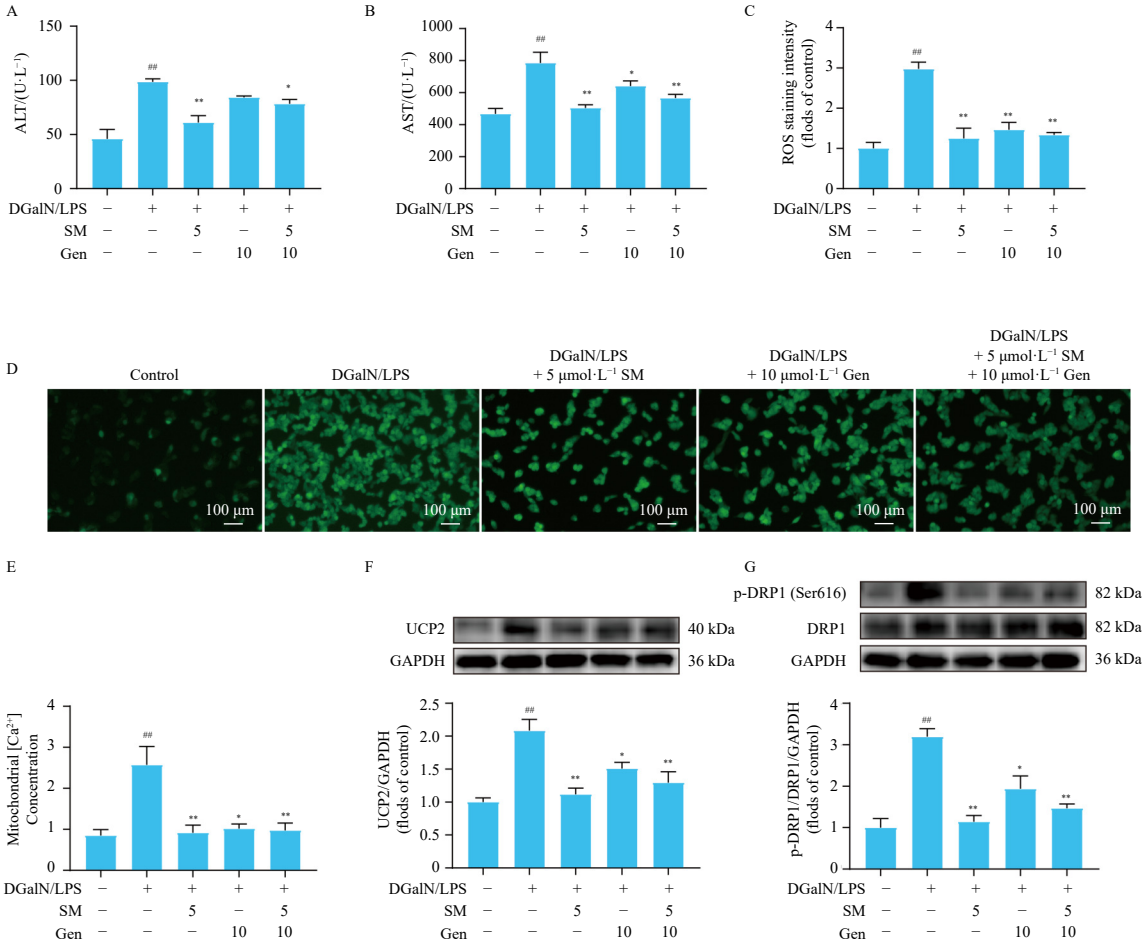

Fig. 9 Inhibition of UCP2 partially attenuated the protective effects of SM against mitochondrial dysfunction *in vitro*. (A–B) ALT and AST levels in HepG2 cells were measured by biochemical assays (n = 6). (C) Quantitative immunofluorescence analysis of ROS staining intensity in HepG2 cells (n = 3). (D) Representative immunofluorescence images of ROS in HepG2 cells (Scale bar = 100 μm) (n = 3). (E) Quantitative immunofluorescence analysis of mitochondrial calcium staining intensity in HepG2 cells (n = 8). (F–G) Protein expression levels of UCP2, p-Drp1, and Drp1 in HepG2 cells were quantitatively analyzed by Western blot (n = 3). Data are shown as mean ± SEM. $^{\#\#}P$ <0.01 *vs* normal group, $^{*}P$ < 0.05, $^{**}P$ < 0.01 *vs* Model group.

stress can trigger mitophagy in a mitochondrial fission-dependent manner [45]. LC3B is a key marker of autophagosome formation and maturation [46], and its interaction with Drp1 may facilitate autophagosome assembly, enhancing cellular stress responses. Drp1, a GTPase, is the primary mediator of mitochondrial fission, with phosphorylation at Ser616 promoting its activation and fission activity. PINK1 acts as a sensor of mitochondrial damage, recruiting Drp1 to dysfunctional mitochondria to initiate fission and subsequent mitophagy [47]. In contrast, MFN2 promotes mitochondrial fusion, and the balance between Drp1 and MFN2 is essential for maintaining mitochondrial dynamics. In this study, TAA-treated mice exhibited upregulated expression of LC3B, PINK1, and p-Drp1 (Figs. 7A–7C and 7E), while MFN2 expression was downregulated (Fig. 7D), consistent with prior reports [48]. SM treatment reversed these alterations. Immunohistochemical analysis further confirmed changes in PINK1, MFN2, and LC3B expression (Figs. 7F–7J), indicating that SM suppresses autophagy activation in HE. Additionally, we found that the UCP2 inhibitor GEN enhanced the antioxidant effects of SM (Figs. 8C–8E). SM treatment significantly reduced UCP2 expression (Fig. 8G), but the combination of SM and GEN did not further reduce UCP2 levels, suggesting that both agents act through a shared pathway. Mitochondrial dysfunction involves impaired bioenergetics, elevated ROS, calcium dysregulation, and disrupted dynamics [49]. Therefore, we assessed ROS, mitochondrial calcium levels, and p-Drp1 in HepG2 cells. *In vitro*, SM reduced ROS and mitochondrial calcium levels compared to the DGalN/LPS group. However, UCP2 inhibition partially reversed SM's suppressive effects on ROS and calcium release (Figs. 9C–9E). Similarly, DGalN/LPS stimulation increased UCP2 expression, which was reduced by SM; this effect was attenuated in the presence of the UCP2 inhibitor. The inhibitory effects of SM on UCP2 and p-Drp1 were also partially reversed (Figs. 9F and 9G). These results strongly suggest that UCP2 is a direct target of SM and that SM exerts neuroprotective and hepatoprotective effects by inhibiting oxidative stress-mediated mitophagy and mitochondrial dysfunction.

5. Conclusions

In conclusion, the results suggest that SM exerts hepatoprotective effects by alleviating oxidative stress and mitochondrial dysfunction. The underlying mechanism may involve suppression of mitophagy through inhibition of UCP2 protein expression, which appears linked to the UCP2/PINK1/Drp1/MFN2/LC3B signaling pathway (Figs. 10). Importantly, these findings indicate that SM could serve as a potential therapeutic agent for HE.

Funding

This work was supported by "the National Science and Technology Major Project" from the Ministry of Science and Technology of the People's Republic of China (No. 2017ZX09301050).

Declaration of Competing Interests

These authors have no conflict of interest to declare.

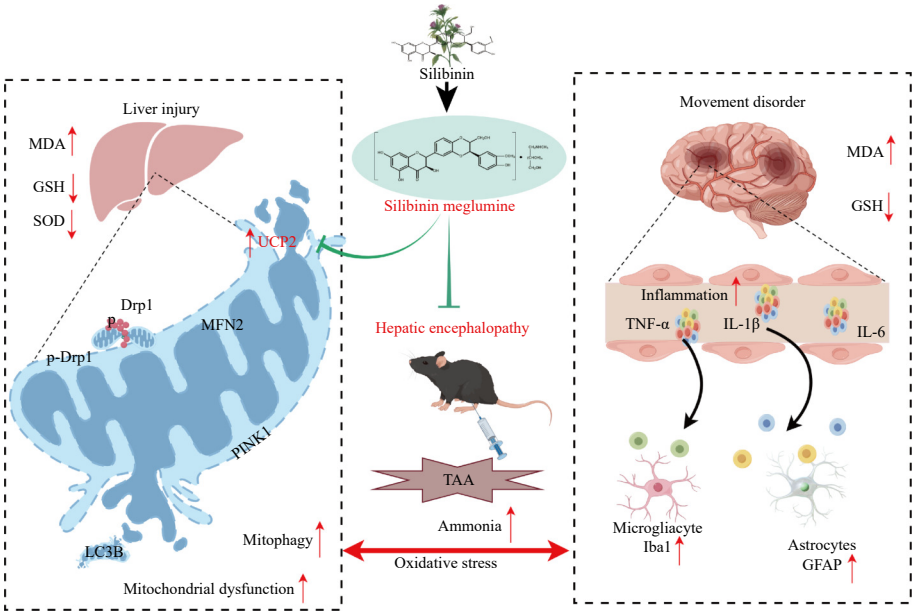

Fig. 10 SM alleviated HE by inhibiting UCP2 expression, thereby reducing oxidative stress-induced mitophagy in mice. In TAA-induced HE mice, SM improved liver function and reduced serum ammonia levels. It also decreased the levels of inflammatory cytokines, including TNF-α and IL-6, in both plasma and brain tissue, lowered the oxidative stress marker MDA, and increased GSH levels. Furthermore, SM downregulated UCP2 expression in liver tissue, thereby alleviating oxidative stress and mitochondrial dysfunction through the UCP2/PINK1/Drp1/MFN2/LC3B pathway, highlighting its potential as a therapeutic agent for HE.

References

1 Häussinger D, Dhiman RK, Felipo V, et al. Hepatic encephalopathy. *Nat Rev Dis Primers*. 2022;8(1):43. https://doi.org/10.1038/s41572-022-00366-6.
2 Louissaint J, Deutsch-Link S, Tapper EB. Changing epidemiology of cirrhosis and hepatic encephalopathy. *Clin Gastroenterol Hepatol*. 2022;20(8S):S1-S8. https://doi.org/10.1016/j.cgh.2022.04.036.
3 Rose CF, Amodio P, Bajaj JS, et al. Hepatic encephalopathy: novel insights into classification, pathophysiology and therapy. *J Hepatol*. 2020;73(6):1526-1547. https://doi.org/10.1016/j.jhep.2020.07.013.
4 Görg B, Karababa A, Schütz E, et al. *O*-GlcNAcylation-dependent upregulation of HO1 triggers ammonia-induced oxidative stress and senescence in hepatic encephalopathy. *J Hepatol*. 2019;71(5):930-941. https://doi.org/10.1016/j.jhep.2019.06.020.
5 Hu C, Zhang X, Wei W, et al. Matrine attenuates oxidative stress and cardiomyocyte apoptosis in doxorubicin-induced cardiotoxicity *via* maintaining AMPKα/UCP2 pathway. *Acta Pharm Sin B*. 2019;9(4):690-701. https://doi.org/10.1016/j.apsb.2019.03.003.
6 Li S, Sun D, Chen S, et al. UCP2-SIRT3 signaling relieved hyperglycemia-induced oxidative stress and senescence in diabetic retinopathy. *Invest Ophthalmol Vis Sci*. 2024;65(1):14. https://doi.org/10.1167/iovs.65.1.14.
7 Padmanaban S, Pully D, Samrot AV, et al. Rising influence of nanotechnology in addressing oxidative stress-related liver disorders. *Antioxidants (Basel)*. 2023;12(7):1405. https://doi.org/10.3390/antiox12071405.
8 Bai Y, Li K, Li X, et al. Effects of oxidative stress on hepatic encephalopathy pathogenesis in mice. *Nat Commun*. 2023;14(1):4456. https://doi.org/10.1038/s41467-023-40081-8.
9 Cui S, Pan XJ, Ge CL, et al. Silybin alleviates hepatic lipid accumulation in methionine-choline deficient diet-induced nonalcoholic fatty liver disease in mice *via* peroxisome proliferator-activated receptor α. *Chin J Nat Med*. 2021;19(6):401-411. https://doi.org/10.1016/S1875-5364(21)60039-0.
10 Liu X, Xia N, Yu Q, et al. Silybin meglumine mitigates CCl_4-induced liver fibrosis and bile acid metabolism alterations. *Metabolites*. 2024;14(10):556. https://doi.org/10.3390/metabo14100556.
11 Bai Y, Bai Y, Wang S, et al. Targeted upregulation of uncoupling protein 2 within the basal ganglia output structure ameliorates dyskinesia after severe liver failure. *Free Radic Biol Med*. 2018;124:40-50. https://doi.org/10.1016/j.freeradbiomed.2018.05.005.
12 Li D, Yu SF, Lin L, et al. Deficiency of leucine-rich repeat kinase 2 aggravates thioacetamide-induced acute liver failure and hepatic encephalopathy in mice. *J Neuroinflammation*. 2024;21(1):123. https://doi.org/10.1186/s12974-024-03125-4.
13 Hassan NF, El-Ansary MR, El-Ansary AR, et al. Unveiling the protective potential of mirabegron against thioacetamide-induced hepatic encephalopathy in rats: insights into cAMP/PPAR-γ/p-ERK1/2/p S536 NF-κB p 65 and p-CREB/BDNF/TrkB in parallel with oxidative and apoptotic trajectories. *Biochem Pharmacol*. 2024;229:116504. https://doi.org/10.1016/j.bcp.2024.116504.
14 Wang Y, Yang Z, Wei Y, et al. Apolipoprotein A4 regulates the immune response in carbon tetrachloride-induced chronic liver injury in mice. *Int Immunopharmacol*. 2021;90:107222. https://doi.org/10.1016/j.intimp.2020.107222.
15 Li Y, Li H, Sun M, et al. Silibinin alleviates acute liver failure by modulating AKT/GSK3β/Nrf2/GPX4 pathway. *Naunyn Schmiedebergs Arch Pharmacol*. 2025;398(6):7625-7639. https://doi.org/10.1007/s00210-024-03760-x.
16 Fan X, Wang X, Hui Y, et al. Genipin protects against acute liver injury by abrogating ferroptosis *via* modification of GPX4 and ALOX15-launched lipid peroxidation in mice. *Apoptosis*. 2023;28(9-10):1469-1483. https://doi.org/10.1007/s10495-023-01867-9.
17 Li Y, Xu J, Chen W, et al. Hepatocyte CD36 modulates UBQLN1-mediated proteasomal degradation of autophagic SNARE proteins contributing to septic liver injury. *Autophagy*. 2023;19(9):2504-2519. https://doi.org/10.1080/15548627.2023.2196876.
18 Zhang Y, Xue W, Zhang W, et al. Histone methyltransferase G9a protects against acute liver injury through GSTP1. *Cell Death Differ*. 2020;27(4):1243-1258. https://doi.org/10.1038/s41418-019-0412-8.
19 Kallergi E, Daskalaki AD, Kolaxi A, et al. Dendritic autophagy degrades postsynaptic proteins and is required for long-term synaptic depression in mice. *Nat Commun*. 2022;13(1):680. https://doi.org/10.1038/s41467-022-28301-z.
20 Endicott SJ, Miller RA. PTEN activates chaperone-mediated autophagy to regulate metabolism. *Autophagy*. 2024;20(1):216-217. https://doi.org/10.1080/15548627.2023.2255966.
21 Liang L, Huan L, Wang J, et al. LncRNA RP11-295G202 regulates hepatocellular carcinoma cell growth and autophagy by targeting PTEN to lysosomal degradation. *Cell Discov*. 2021;7(1):118. https://doi.org/10.1038/s41421-021-00339-1.
22 Zhang L, Zhu Z, Yan H, et al. Creatine promotes cancer metastasis through activation of Smad2/3. *Cell Metab*. 2021;33(6):1111-1123. https://doi.org/10.1016/j.cmet.2021.03.009.
23 Chen S, Ma X, Liu Y, et al. Creatine promotes endometriosis by inducing ferroptosis resistance *via* suppression of PRP. *Adv Sci (Weinh)*. 2024;11(38):e2403517. https://doi.org/10.1002/advs.202403517.
24 Montagnese S, Lauridsen M, Vilstrup H, et al. A pilot study of golexanolone, a new GABA-A receptor-modulating steroid antagonist, in patients with covert hepatic encephalopathy. *J Hepatol*. 2021;75(1):98-107. https://doi.org/10.1016/j.jhep.2021.03.012.
25 Munson MJ, Mathai BJ, Ng MYW, et al. GAK and PRKCD kinases regulate basal mitophagy. *Autophagy*. 2022;18(2):467-469. https://doi.org/10.1080/15548627.2021.2015154.
26 Gardin A, Remih K, Gonzales E, et al. Modern therapeutic approaches to liver-related disorders. *J Hepatol*. 2022;76(6):1392-1409. https://doi.org/10.1016/j.jhep.2021.12.015.
27 GBD 2017 Cirrhosis Collaborators. The global, regional, and national burden of cirrhosis by cause in 195 countries and territories, 1990-2017: a systematic analysis for the Global Burden of Disease Study 2017. *Lancet Gastroenterol Hepatol*. 2020;5(3):245-266. https://doi.org/10.1016/S2468-1253(19)30349-8.
28 Lam P, Cheung F, Tan HY, et al. Hepatoprotective effects of Chinese medicinal herbs: a focus on anti-inflammatory and anti-oxidative activities. *Int J Mol Sci*. 2016;17(4):465. https://doi.org/10.3390/ijms17040465.
29 Yang Q, Tan T, He Q, et al. Combined amphiphilic silybin meglumine nanosuspension effective against hepatic fibrosis in mice mode. *Int J Nanomed*. 2023;18:5197-5211. https://doi.org/10.2147/IJN.S407762.
30 Ding Y, Zhang S, Sun Z, et al. Preclinical validation of silibinin/albumin nanoparticles as an applicable system against acute liver injury. *Acta Biomater*. 2022;146:385-395. https://doi.org/10.1016/j.actbio.2022.04.021.
31 Yang J, Sun Y, Xu F, et al. Silibinin protects rat pancreatic β-cell through up-regulation of estrogen receptors' signaling against amylin- or Aβ1-42-induced reactive oxygen species/reactive nitrogen species generation. *Phytother Res*. 2019;33(4):998-1009. https://doi.org/10.1002/ptr.6293.

32 Wu X, Chen J, Ping K, et al. Silybin mitigated liver and brain damage after difenoconazole exposure: crosstalk between oxidative stress, inflammation, ferroptosis and apoptosis. *Pestic Biochem Physiol*. 2024;202:105942. https://doi.org/10.1016/j.pestbp.2024.105942.

33 Selc M, Macova R, Babelova A. Novel strategies enhancing bioavailability and therapeutical potential of silibinin for treatment of liver disorders. *Drug Des Devel Ther*. 2024;18:4629-4659. https://doi.org/10.2147/DDDT.S483140.

34 Rahman TM, Hodgson HJ. The effects of early and late administration of inhibitors of inducible nitric oxide synthase in a thioacetamide-induced model of acute hepatic failure in the rat. *J Hepatol*. 2003;38(5):583-590. https://doi.org/10.1016/S0168-8278(03)00050-3.

35 Abo El-Magd NF, El-Kashef DH, El-Sherbiny M, et al. Hepatoprotective and cognitive-enhancing effects of hesperidin against thioacetamide-induced hepatic encephalopathy in rats. *Life Sci*. 2023;313:121280. https://doi.org/10.1016/j.lfs.2022.121280.

36 Eraky SM, El-Kashef DH, El-Sherbiny M, et al. Naringenin mitigates thioacetamide-induced hepatic encephalopathy in rats: targeting the JNK/Bax/caspase-8 apoptotic pathway. *Food Funct*. 2023;14(2):1248-1258. https://doi.org/10.1039/d2fo03470k.

37 Tamnanloo F, Ochoa-Sanchez R, Oliveira MM, et al. Multiple ammonia-induced episodes of hepatic encephalopathy provoke neuronal cell loss in bile-duct ligated rats. *JHEP Rep*. 2023;5(12):100904. https://doi.org/10.1016/j.jhepr.2023.100904.

38 Tan ZK, Chen LF, Ye ZQ, Lu QP. Xiaohuang Qudan decoction alleviates ANIT-induced cholestatic liver injury by inhibiting the JAK2/STAT3 pathway and regulating TH17/Treg. *Chin J Nat Med*. 2025;23(4):457-470. https://doi.org/10.1016/S1875-5364(25)60854-5.

39 Niu TL, Zhu YM, Mou MJ, et al. Identification of natural product-based drug combination (NPDC) using artificial intelligence. *Chin J Nat Med*. 2025;23(11):1377-1390. https://doi.org/10.1016/S1875-5364(25)60942-3.

40 Jalan R, Rose CF. Heretical thoughts into hepatic encephalopathy. *J Hepatol*. 2022;77(2):539-548. https://doi.org/10.1016/j.jhep.2022.03.014.

41 Matyas C, Haskó G, Liaudet L, et al. Interplay of cardiovascular mediators, oxidative stress and inflammation in liver disease and its complications. *Nat Rev Cardiol*. 2021;18(2):117-135. https://doi.org/10.1038/s41569-020-0443-5.

42 Kumar R, T A, Singothu S, et al. Uncoupling proteins as a therapeutic target for the development of new era drugs against neurodegenerative disorder. *Biomed Pharmacother*. 2022;147:112656. https://doi.org/10.1016/j.biopha.2022.112656.

43 Rangarajan S, Locy ML, Chanda D, et al. Mitochondrial uncoupling protein-2 reprograms metabolism to induce oxidative stress and myofibroblast senescence in age-associated lung fibrosis. *Aging Cell*. 2022;21(9):e13674. https://doi.org/10.1111/acel.13674.

44 Ogando DG, Choi M, Shyam R, et al. Ammonia sensitive SLC4A11 mitochondrial uncoupling reduces glutamine induced oxidative stress. *Redox Biol*. 2019;26:101260. https://doi.org/10.1016/j.redox.2019.101260.

45 Baechler BL, Bloemberg D, Quadrilatero J. Mitophagy regulates mitochondrial network signaling, oxidative stress, and apoptosis during myoblast differentiation. *Autophagy*. 2019;15(9):1606-1619. https://doi.org/10.1080/15548627.2019.1591672.

46 Hwang HJ, Ha H, Lee BS, et al. LC3B is an RNA-binding protein to trigger rapid mRNA degradation during autophagy. *Nat Commun*. 2022;13(1):1436. https://doi.org/10.1038/s41467-022-29139-1.

47 Gao Q, Tian R, Han H, et al. PINK1-mediated Drp1(S616) phosphorylation modulates synaptic development and plasticity *via* promoting mitochondrial fission. *Signal Transduct Target Ther*. 2022;7(1):103. https://doi.org/10.1038/s41392-022-00933-z.

48 Jacob S, Kosaka Y, Bhatlekar S, et al. Mitofusin-2 regulates platelet mitochondria and function. *Circ Res*. 2024;134(2):143-161. https://doi.org/10.1161/CIRCRESAHA.123.322914.

49 Zong Y, Li H, Liao P, et al. Mitochondrial dysfunction: mechanisms and advances in therapy. *Signal Transduct Target Ther*. 2024;9(1):124. https://doi.org/10.1038/s41392-024-01839-8.